A mass-conserving fast algorithm to parameterize gravitational transport and deposition using digital elevation models

S. Gruber[1,2]

Received 8 January 2006; revised 4 January 2007; accepted 13 March 2007; published 14 June 2007.

[1] Many natural phenomena such as snow avalanches, debris flows, or lahars involve gravitational transport and deposition that is largely governed by topography. This paper describes a fast and mass-conserving algorithm to parameterize mass transport and deposition (MTD) over a digital elevation model. The algorithm is an extension to existing flow-routing and terrain parameterization techniques. Its fast execution allows application over large areas or its incorporation into other models, e.g., distributed glacier mass balance in mountain topography. The proposed method does not include effects of kinetic energy and thus neglects potential uphill flow of fast-moving mass. The application of MTD is described at the example of small and frequent snow avalanches in steep terrain for which the required parameters are approximated from published data. The algorithm MTD has been developed and is described for the gravitational redistribution of snow, but it is also applicable to other types of mass movements.

Citation: Gruber, S. (2007), A mass-conserving fast algorithm to parameterize gravitational transport and deposition using digital elevation models, *Water Resour. Res.*, *43*, W06412, doi:10.1029/2006WR004868.

1. Introduction

[2] Many phenomena that are simulated using digital elevation models (DEMs) involve gravitational transport and deposition. Depending on the task at hand, investigation and modeling of these phenomena can cover diverse spatial scales and levels of sophistication. Especially in geographic information system (GIS) environments, process models are often impractical to use because of their requirements in terms of computing resources or input data, but simple algorithms of both transport and deposition are rare. For this reason, several studies employ work-around techniques: Hazard potentials of debris flows or ice avalanches have been assessed using flow propagation schemes and a runout distance determined by a limiting value for the average slope between the starting zone and the lowest potential deposit [*Huggel et al.*, 2003, 2004; *Salzmann et al.*, 2004; *Noetzli et al.*, 2006]. In the Alpine permafrost model PERMAKART [*Keller*, 1992], locations of avalanche deposits are determined rule-based using terrain curvature and slope. The model LAHARZ [*Iverson et al.*, 1998] propagates lahar flows over a DEM until the flow stops by mass depletion. The geomorphological model LAPSUS uses path length and runout distance [*Claessens et al.*, 2006] or different capacities for transport, detachment, and settlement [*Schoorl et al.*, 2002] in a multiple flow-direction algorithm to determine deposition. Both applications are rare examples of transport and deposition in a GIS-like environment. Other approaches such as a mass-conserving algorithm used in a dynamic model of talus-derived rock glacier occurrence [*Frauenfelder*, 2004] or a model of glacier flow and extent in paleoclimates [*Plummer and Phillips*, 2003] exist but are less suitable for generalization to other problems.

[3] The model proposed in this paper was developed in the context of the distributed modeling of Alpine glacier mass balance [for a first application, see *Machguth et al.*, 2006] and ground temperatures where snow transport and deposition by avalanches is of great importance [*Haeberli*, 1975; *Gruber-Schmid and Sardemann*, 2003; *Kaser et al.*, 2003; *Gruber*, 2005]. It achieves a simple parameterization of gravitational redistribution of mass in mountainous terrain and is computationally much less intense than dynamic avalanche models [e.g., *Naaim and Ancey*, 1992; *Sampl and Zwinger*, 2004]. It is a parameterization model because the physics of flow and deposition are not explicitly considered but characterized by simple parameters. Mass flow is achieved on the basis of common assumptions of flow routing on regular DEMs, and deposition is controlled only by the available mass and a maximum deposition that is a local variable. The name MTD derives from mass transport and deposition. The algorithm is described in a generic way but evaluated using examples of small high-frequency snow avalanches in steep topography.

2. Method

2.1. Combining Transport and Deposition

[4] Mobile mass M is moved downslope. In each cell, the fraction off mass f_{NB} drained to neighbor NB is a function of topography only and must sum to one over all neighboring cells in order to preserve mass. Deposition D is limited by the local maximum deposition D_{max} and the available mobile mass M that is the sum of initial input I and received

[1]Department of Geography, University of Zurich, Zurich Switzerland.
[2]Laboratoire des Environnements, Dynamiques et Territoires de la Montagne, Université de Savoie, Le Bourget du Lac, France.

0043-1397/07/2006WR004868

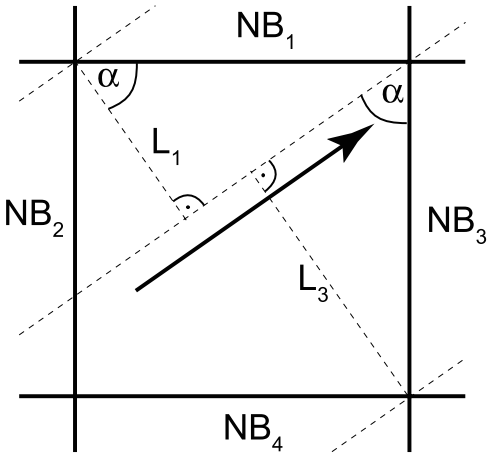

Figure 1. Terminology and flow apportioning method. The cardinal neighbors are designated NB_1 to NB_4; the projected flow widths into them are L_1 to L_4; and the aspect α is given in degrees clockwise from north and indicated by the arrow.

flow R from the neighboring cells. The flow F_{NB} into each neighbor NB is given by the mass remaining after deposition M-D and the draining fractions f_{NB}. D_{max} is independent of the mass flux and a function of, e.g., slope angle or surface characteristics, that needs to be derived empirically.

$$D = \begin{cases} M & \text{if } M < D_{max}, \\ D_{max} & \text{if } M \geq D_{max}. \end{cases} \quad (1)$$

$$F_{NB} = (M - D) \cdot f_{NB} \quad (2)$$

[5] Regular grids of elevation z, initial mass I, and maximum deposition D_{max} are required for the model. Equally sized arrays of deposition D and mobile mass M are computed. The following sections discuss the mechanisms of transport and of deposition in more detail.

2.2. Transport Mechanism

2.2.1. General Considerations

[6] The potential flow from one cell into its neighbors is exclusively dependent on topography. Only the elevation differences between cells (i.e., potential energy) is used in the flow propagation scheme, and kinetic energy is entirely neglected. No mass is propagated over horizontal areas or uphill. A large number of different approaches for flow propagation in GIS and similar grid-based modeling tools as well as corresponding evaluations have been published [e.g., *O'Callaghan and Mark*, 1984; *Lea*, 1992; *Quinn et al.*, 1991; *Freeman*, 1991; *Holmgren*, 1994; *Tarboton*, 1997]. Three types of grid-based algorithms are available: (1) single-neighbor methods [*O'Callaghan and Mark*, 1984; *Lea*, 1992] that route all mass from one cell into only one neighboring cell; (2) single-direction multiple-neighbor methods [*Tarboton*, 1997] that utilize a single flow direction and resolve this by apportioning mass to two adjacent cells if the flow direction is not a multiple of 45°, and (3) multiple flow-directions methods [*Quinn et al.*, 1991; *Freeman*, 1991; *Holmgren*, 1994] in which all lower neighbors receive mass. In principle, any of these methods can be extended with a deposition function, but some are more suitable for this application than others. Single-neighbor methods fail to capture diverging flow that occurs on convex terrain. Multiple flow-direction methods propagate a small proportion of mass to all lower neighbors, i.e., also nearly horizontal laterally, and for this reason, a single-direction multiple-neighbor technique is preferred for MTD in order to allow for divergent flow and, at the same time, to constrain overdispersion. This type of method involves the two steps of (1) determining the aspect or flow direction of each cell; and (2) the apportioning of flow between two cells if the flow direction is not directly toward the center of one neighbor. Since a plane is uniquely defined by three points, the determination of aspect on a rectangular grid based on more than three points always involves inconsistencies. This may lead to two pixels draining into each other (i.e., uphill or horizontal flow) and needs to be corrected in order to keep a consistent flow and to preserve mass.

2.2.2. Derivation of the Flow Field

[7] The method proposed here resolves the slight ambiguity of flow apportioning inherent in, e.g., the $D\infty$ algorithm [*Tarboton*, 1997]. The aspect angle α is determined following the common approach of *Evans* [1972]. On the basis of the aspect, the fraction of flow f_{NB} to each cardinal neighboring cell NB is computed.

[8] By using only cardinal and no diagonal cells (that have no actual connection to the center cell permitting flow), the flow width into each cell L_{NB} can be determined by projecting the pixel sides onto the normal to the aspect vector (see Figure 1). The use of only four cardinal neighbors is computationally faster than the use of all eight surrounding cells but also results in a larger lateral dispersion caused by the spatial discretization. In pronounced terrain, this effect is likely of minor importance.

$$L_1 = \cos(\alpha) \cdot cs \quad (3)$$

$$L_2 = -\sin(\alpha) \cdot cs \quad (4)$$

$$L_3 = \sin(\alpha) \cdot cs \quad (5)$$

$$L_4 = -\cos(\alpha) \cdot cs \quad (6)$$

The flow widths L_{NB} are derived on the basis of the aspect angle α and the cell size cs and corrected for horizontal or uphill flow (Δz is defined by the elevation of the center cell minus the elevation of neighbor NB) that can result from the inconsistency in determining the aspect on a rectangular grid as well as for negative values of L_{NB} received by uphill pixels

$$C_{NB} = L_{NB} \cdot H(\Delta z) \cdot H(L_{NB}) \quad (7)$$

using the step function $H(X)$:

$$H(X) = \begin{cases} 1 & \text{if} \Delta z > 0, \\ 0 & \text{if} \Delta z \leq 0. \end{cases} \quad (8)$$

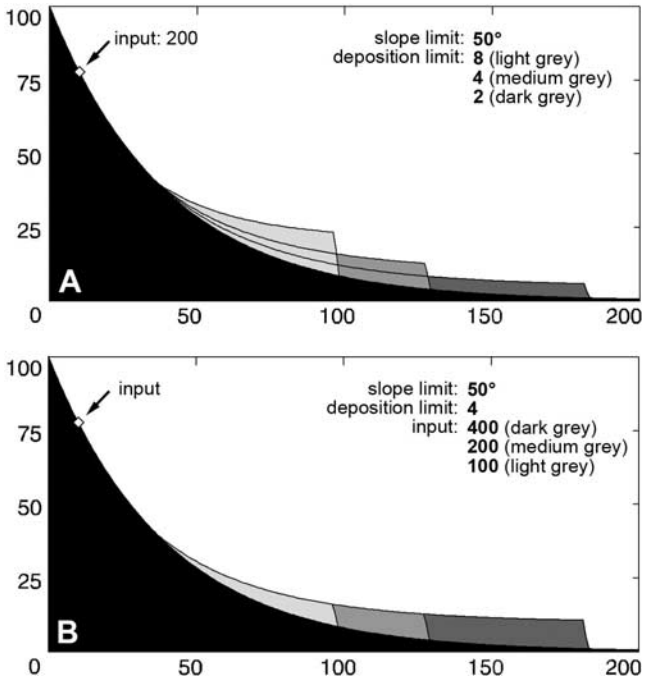

Figure 2. One-dimensional example of deposition resulting from the simple parameterization using $D_{\lim}$ and $\beta_{\lim}$. (a) Increasing the deposition limit $D_{\lim}$ results in thicker deposition further upslope. (b) More mass input results in further propagation toward lower slopes but identical deposition further upslope when both $D_{\lim}$ and $\beta_{\lim}$ are fixed. Deposits in darker shades extend also behind lighter grey. Both vertical and horizontal axes are units of distance, input has units of mass, and the deposition limits are given as unit mass per unit length. An unnatural slope limit $\beta_{\lim}$ =50° has been chosen to make a more comprehensible figure.

The fractions f_{NB} draining into each neighbor NB are obtained by normalization over all corrected flow widths C_{NB} in oder to preserve mass

$$f_{NB} = \frac{C_{NB}}{C_1 + C_2 + C_3 + C_4}. \quad (9)$$

2.3. Deposition Mechanism

[9] Only local characteristics determine maximum deposition $D_{\max}$, which in this model is assumed to be independent of the amount of transported mass. For a constant terrain geometry, this also relates events of differing magnitude to different runout distances. However, these will be different for events of equal magnitude but variable path and deposition geometry. Deposition in channel, for instance, will result in larger runout than on a convex fan with divergent flow. A simple function is used here to relate $D_{\max}$ to the local slope angle β that is assumed to be its most important determinant:

$$D_{\max} = \begin{cases} \left(1 - \frac{\beta}{\beta_{\lim}}\right) \cdot D_{\lim} & \text{if } \beta < \beta_{\lim}, \\ 0 & \text{if } \beta \geq \beta_{\lim}. \end{cases} \quad (10)$$

$D_{\lim}$ is the limiting deposition, i.e., the maximum deposition that would occur on horizontal terrain. The limiting slope $\beta_{\lim}$ denotes the maximum terrain steepness at which some mass is deposited and is related to the angle of repose for the transported material. Figure 2 illustrates the effect that changes in $D_{\lim}$ and the amount of transported mass have on deposition. Where more detailed information is available, the determination of $D_{\max}$ can also include a more complicated function of slope or information such as surface characteristics, curvature, or local features such as dams.

2.4. Sources of Transported Material

[10] Material to be transported is supplied as a grid in which each cell has a value that corresponds to the amount of material that is available, specified as unit mass per unit area, e.g., kg/m^2. This can be achieved by considering one cell as a point source for, e.g., debris flows originating from lake outburst [*Huggel et al.*, 2003] or lahars [*Iverson et al.*, 1998]. Larger areas that yield transportable material can also be specified for, e.g., snow avalanches [*Gruber-Schmid and Sardemann*, 2003; *Maggioni and Gruber*, 2003]. Sediment entrainment along the flow path is often very important [e.g., *Sovilla et al.*, 2001], but since this parameterization model does not include dynamic processes, it can only be specified in input grid together with the original release input.

3. Implementation

3.1. Topography Initialization

[11] The four draining fractions f_{NB} as well as the index to access the grids in the order of descending elevation are precomputed and stored for later propagation calculations. If the topography and hence the flow field does not change significantly between mass propagation events, the same precomputed values can be used. If previous deposition can affect the mass flow, the topography needs to be updated, and the flow field needs to be reinitialized (and possibly $D_{\max}$ recomputed). Only a DEM and the cell size are needed as input. During initialization, iterative sink filling and correction of horizontal areas [*Garbrecht and Martz*, 1997] is applied (adjusted to evaluate and correct only cardinal neighbors) in order to prevent mass loss in sinks or horizontal areas.

3.2. Mass Propagation

[12] Gridded data of input mass I and maximum deposition $D_{\max}$ (both in units of mass per unit of area) as well as the precomputed flow field need to be supplied for propagation. The algorithm loops through all cells in the order of descending elevation and, for each cell that contains mass, computes deposition and updates M of neighboring cells if they receive mass. Grids of deposition D and mobile mass M are computed. The sum of grids D and M describes the amount of mass that has been present in each cell. After computation, the total of the input I equals the total of the deposition D. Exception to this is the transport of material out of the model domain if this does not include all relevant deposition areas or the loss of mass if sinks where $M > D_{\max}$ were not removed.

3.3. Double-Resolution Computation

[13] While the flow propagation only to cardinal neighbors is less ambiguous in the partitioning of flow between cells adjacent to the flow direction, it also has the disadvantage of producing a coarser flow pattern or to result in excessive sink filling in narrow channels. Depending on the application and the resolution of the DEM used, this can be overcome by resampling the model data to double spatial

Figure 3. View from the Mont Blanc massif into the Swiss Alps. Large dark areas of steep and snow-free slopes stand out in the generally snow covered landscape. The snow from these slopes is transferred to lower areas by small but frequent avalanches.

resolution before computation and aggregation of results afterward. Using double resolution, ridge pixels contribute mass to two sides. Otherwise this would only be possible with multiple flow-direction methods but not with single flow-direction multiple-neighbor methods. Double-resolution computation requires about four times more computing time than original resolution. The spatial grid size of input and output remains unchanged, and only internal processing is performed at higher resolution.

4. Model Evaluation at the Example of Snow Redistribution in Steep Topography

[14] The model MTD is demonstrated and evaluated using snow redistribution by small and frequent avalanches in Alpine terrain. The importance of this process can be inferred from Figures 3 and 4. While several researchers stress the importance of wind redistribution in complex terrain and develop corresponding algorithms [e.g., *Purves et al.*, 1999; *Winstral et al.*, 2002] the effect of avalanches is usually not considered. This may be due to a sampling bias, as accessible and measured locations for snow height or mass balance usually are in safe terrain where the effect of wind redistribution dominates. Considering the difficulty of computing realistic wind fields in complex terrain [cf. *Lehning et al.*, 2000], the parameterization of gravitational redistribution of snow as proposed here can improve snow distribution patterns greatly with relative computational ease. A first application is shown in the study of *Machguth et al.* [2006].

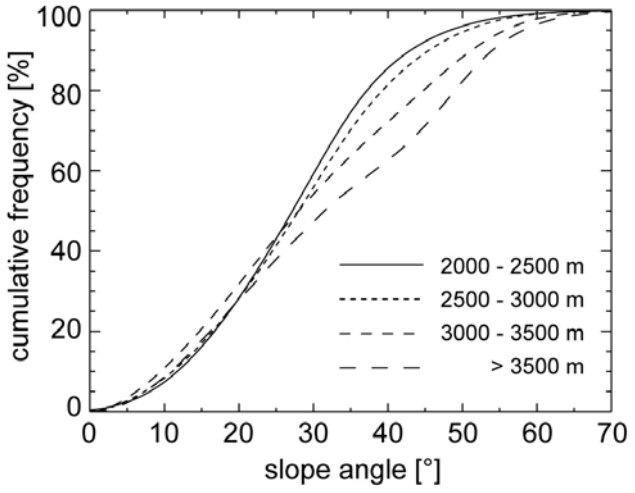

Figure 4. Cumulative frequency distribution of slope steepness for different elevation zones of the Swiss Alps. The glacial equilibrium line is usually situated between 2700 and 3300 m.a.s.l. Thus about one fourth to one third of the glacial accumulation areas comprises slopes steeper than 40° where frequent redistribution by avalanches is likely. Data source: 25-m DEM of the Swiss Federal Office of Topography.

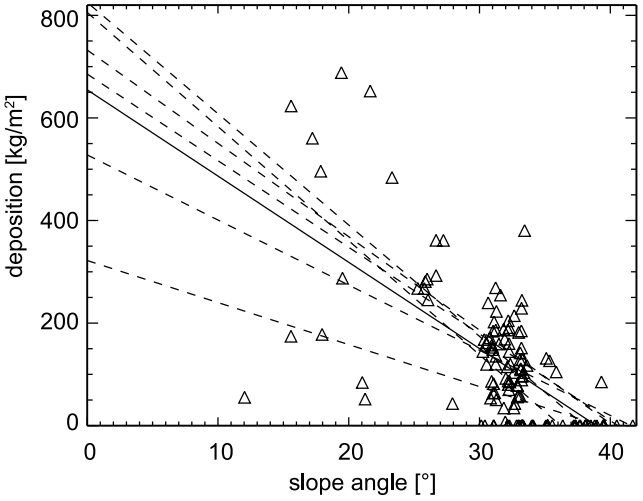

Figure 5. Measured deposition as a function of slope for all six Pizzac avalanches (triangles). Dashed lines are fitted to individual events; the continuous line is fitted to all data points.

4.1. Parameter Values

[15] Useful parameter ranges for β_{lim} and D_{lim} as applicable for small and frequent avalanches need to be estimated prior to model evaluation. Data of six small avalanche events [*Sovilla et al.*, 2001; *Sovilla*, 2004] from the Italian Dolomites were used for this. In the original publication, all events are classified as dense avalanches and occurred in the same channel; their absolute and relative (with respect to other events in the same channel) sizes are small except for the events of 21 December 1997 and 5 March 1999 that were considered to have medium relative size. For each event as well as for all events together, D_{lim} and β_{lim} were determined by linear regression (Table 1 and Figure 5) using the x intercept of the resulting line for β_{lim} and the y intercept for D_{lim}. The high-resolution slope measurements were interpolated and smoothed with a 50-m running mean prior to data analysis.

[16] The estimated parameter ranges are 36° to 41° with a mean of 39° for β_{lim} and 320 to 825 kg/m^2 with a mean of 655 kg/m^2 for D_{lim}. It must be kept in mind that this set of parameters is used for model demonstration and that differing parameters may be obtained by fitting the model to events on open slopes or with different event sizes or snow characteristics. Ideally, multiple events from different sites should be used to avoid the bias that is likely inherent in this

Table 1. Summary of the Pizzac Avalanche Data Used

Event	Reference	Typology	Maximum Mass, 10^3 kg	Runout Distance, m	Data Points	R^2	β_{lim}, degrees	D_{lim}, kg/m^2
5 December 1997	*Sovilla* [2004], *Sovilla et al.* [2001]	Dry	61	547	21	0.44	41	685
21 December 1997	*Sovilla* [2004], *Sovilla et al.* [2001]	Dry	505	680	31	0.73	36	805
14 April 1998	*Sovilla* [2004], *Sovilla et al.* [2001]	Moist	126	530	16	0.16	39	320
28 April 1998	*Sovilla* [2004], *Sovilla et al.* [2001]	Wet	296	540	15	0.52	38	825
11 January 1999	*Sovilla* [2004]	Dry	167	555	26	0.56	40	730
5 March 1999	*Sovilla* [2004]	Dry	468	753	26	0.22	41	525
All Events					135	0.43	39	655

analysis that had to be based on data from only one channel because of the sparsity of information on small avalanches or snow slides.

4.2. Model Demonstration

[17] MTD is demonstrated using the catchment of the small Swiss glacier Vadret da Misaun (9°53′E, 46°25′N) and a hypothetical situation of snow cover and avalanche transport. The parameter values obtained from the Pizzac avalanche (small, channeled) are used in first approximation despite slightly different characteristics here. A uniform snow height of h = 0.5 m and snow density of ρ = 130 kg/m^3 is assumed. Using the 25-m DEM of the Swiss Federal Office of Topography, the slope β is lower than 65° in the test area. For this evaluation, the amount of transported snow I in kg/m^2 is determined as a function of slope

$$I = \begin{cases} 0 & \text{if } \beta < 40^\circ, \\ h \cdot \rho \frac{\beta - 30}{50} & \text{if } \beta \geq 40^\circ. \end{cases} \quad (11)$$

resulting in I to be between 13 and 45.5 kg/m^2 for slopes steeper than 40°. The remaining snow cover R in kg/m^2 is computed as $h \cdot \rho - I$. Figure 8 shows the snow cover per area T in kg/m^2 after transport and deposition given by the

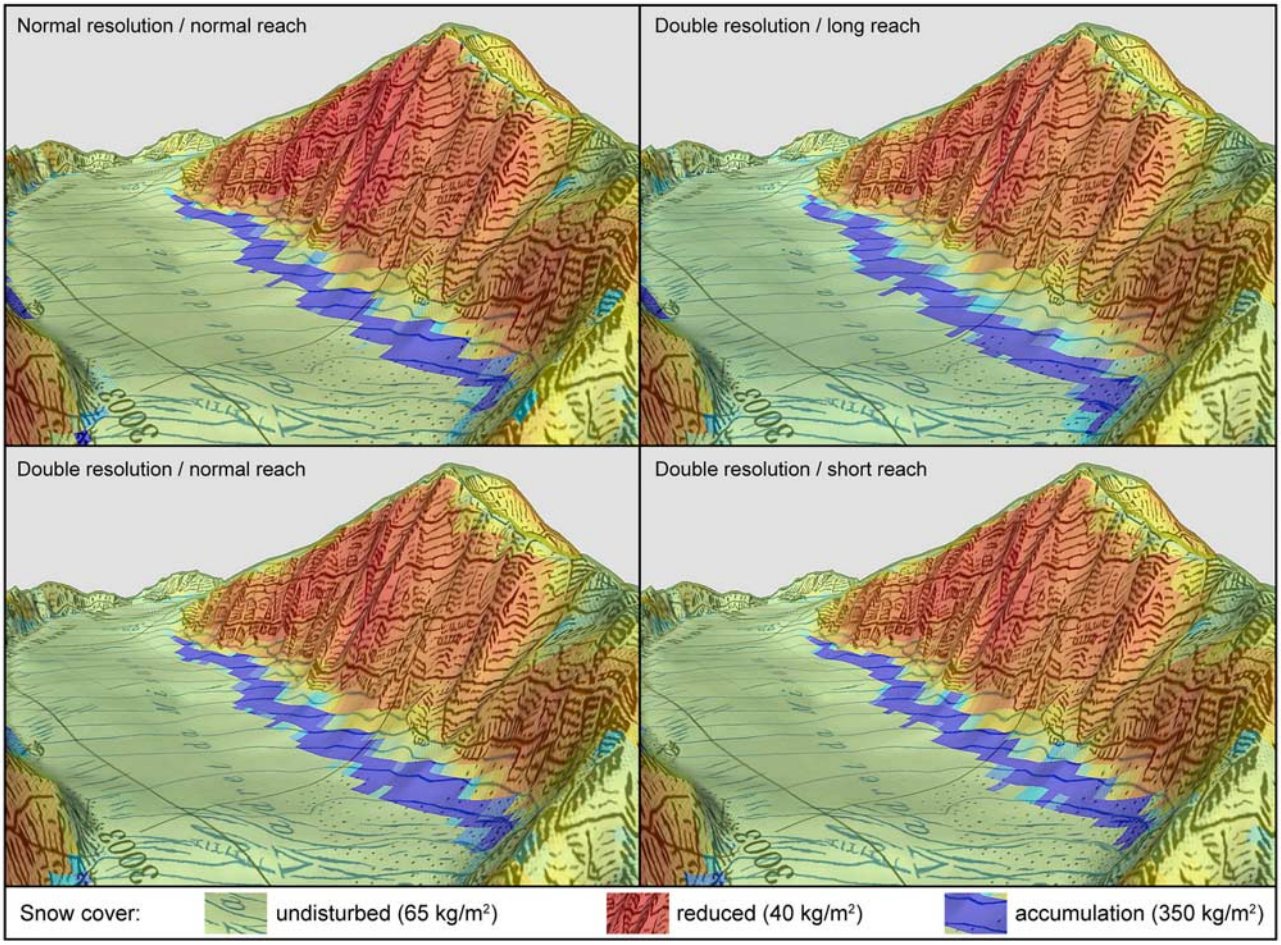

Figure 6. Snow cover after transport and deposition using different cell sizes, normal resolution computation and the mean values β_{lim} = 39° and D_{lim} = 655 kg/m^2. See Figure 7 for color legend. A scanned 1:25,000 topographic map is used as image texture in addition to colors representing snow cover. Reproduced by permission of swisstopo (BA071165).

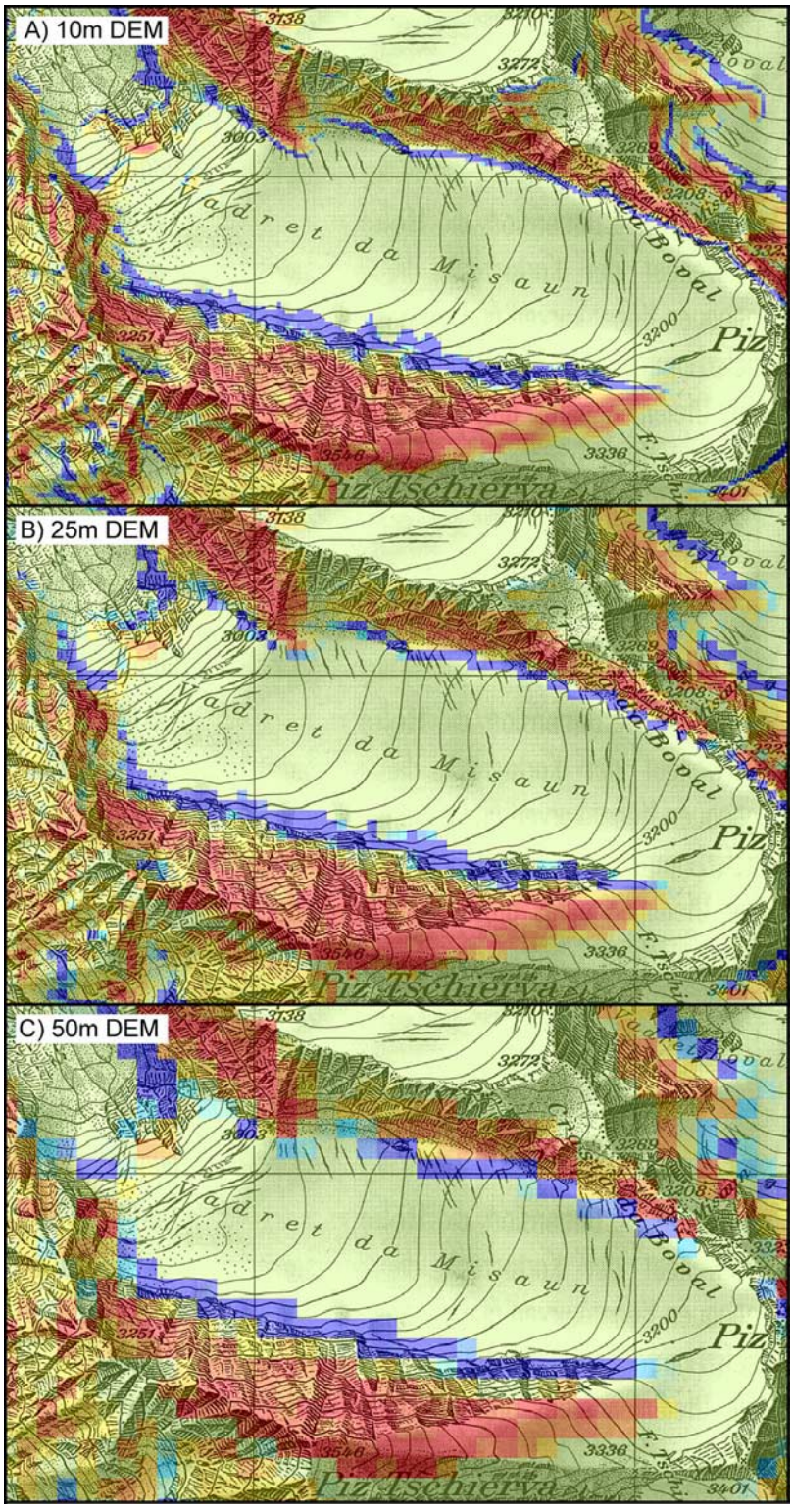

Figure 7. Comparison of snow cover resulting from model runs using 10-m, 25-m, and 50-m cell size DEMs. Data have been aggregated to a common cell size of 50 m for this scatterplot. Reproduced by permission of swisstopo (BA071165).

sum of the remaining snow cover and the calculated deposition $T = R + D$.

[18] A higher mass input, a lower limiting slope β_{lim}, and lower limiting deposition D_{lim} all result in longer reach (or runout) of an event (cf. also Figures 2 and 7).

4.3. Sensitivity to Cell Size

[19] In addition to the basic model behavior illustrated by Figures 2 and 6, Figure 7 illustrates the influence that the cell size has on the results of MTD. For this purpose, the

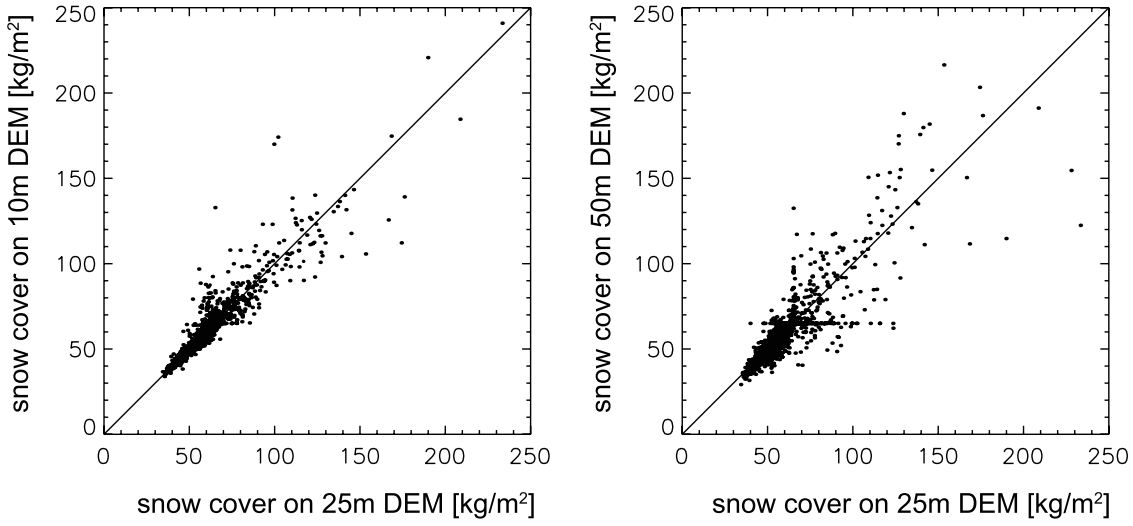

Figure 8. Snow cover after transport and deposition using different model parameters and normal- versus double-resolution computation. Deposition at the glacier edge at the foot of slope is visible as well as a slight shift of the deposition area upslope for "short reach" and downslope for "long reach" settings. The parameters of β_{lim} and D_{lim} were varied based on the values determined in section 4.1. Normal reach refers to the mean values $\beta_{lim} = 39°$ and $D_{lim} = 655$ kg/m^2. Long reach is given by the minimal values of $\beta_{lim} = 36°$ and $D_{lim} = 320$ kg/m^2, and short reach is given by the maxima of $\beta_{lim} = 41$ and $D_{lim} = 825$ kg/m^2. A scanned 1:25,000 topographic map is used as image texture in addition to colors representing snow cover.

25-m DEM has been resampled to 10-m resolution using cubic convolution [*Park and Schowengerdt*, 1983] and aggregated to 50 m by averaging. For all the DEMs (original, increased, and degraded resolutions), the same experiment as in the preceding section has been conducted, and the results are shown in Figure 7. While higher resolution can resolve details such as gullies or narrow deposition zones, the overall picture and spatial context of deposition remains constant between the three DEMs used. Figure 8 shows scatterplots that compare the results of all three DEMs after aggregation to a common cell size of 50 m.

4.4. Sensitivity to Time Stepping

[20] MTD is intended to be used for more than just application to single events. If it is run in a transient model of, e.g., mass and energy balance in steep topography also, its temporal scaling behavior needs to be considered. Time stepping in the model will almost certainly differ from the wide range of occurrence intervals encountered in nature that ranges from minutes for spindrift to years for large avalanches. When using MTD, the time step needs to be consistent in its relation with D_{lim}. Assuming a constant snow fall rate and constant production of transportable mass, a doubling time interval between transport calculations results in doubled available mass and thus longer runout when the same D_{lim} is used. This can be overcome by introducing time into D_{lim} and considering it a limiting deposition rate in kg m^{-2} s^{-1}.

5. Conclusion and Outlook

[21] MTD is a relatively simple and computationally light method for the transport and deposition of mass over a DEM. Its basic principle can be applied easily in flow routing schemes other than the one presented here (e.g., $D\infty$ or MFD). It is mass-conserving when used with a DEM that includes the entire deposition area. If a DEM contains steep slopes over which transport occurs but lacks the downslope deposition area, the corresponding mass is lost from the model domain (in agreement with reality). MTD has been developed for snow redistribution in a model of mass and energy balance in rugged terrain. Application to other gravitational phenomena such as debris flows, ice avalanches, lahars, or erosion and deposition of soil is possible if appropriate parameter values are found (empirically or by using physics-based dynamic models of the process investigated). The benefits and limitations should be carefully considered: MTD is fast by comparison with other physics-based models that need to evaluate more quantities during computation and can be applied to large areas quickly. However, because of the neglect of kinetic energy, upslope movement of a fast flow cannot be modeled. This drawback is common to most other simple parameterizations of flow over DEMs [cf. *Huggel et al.*, 2003; *Iverson et al.*, 1998]. Furthermore, erosion along the path of a mass movement is not accomplished with this model, although in many cases this may be of importance [cf. *Sovilla et al.*, 2001; *Sovilla*, 2004] to the total mass and runout distance of the event. The influence of artifacts and uncertainty in a DEM can be evaluated and minimized using Monte Carlo methods [*Hengl et al.*, 2004] as many realisations of MTD can be calculated over a DEM with artificially added noise (random or conditional simulation). Similarly, a measure of probability (for, e.g., inundation or deposition of a certain mass) can be derived from multiple realizations if the statistical distribution of events that result in transport and deposition is known or can be estimated. Between individual episodes of transport and deposition (e.g., two avalanches,

two debris flows), the topography can be updated in order to reflect the changes in surface elevation caused by deposition.

[22] **Acknowledgments.** Betty Sovilla from the Swiss Federal Institute for Snow and Avalanche Research has kindly made available the Pizzac avalanche data and provided valuable advice. The flow routing method has been inspired by the Mass-Flux Method by Scott Peckham implemented in RiverTools™. This work has been supported by the Swiss National Science Foundation grants 21-63678 and 200020-100222 as well as a postdoctoral fellowship of the French Ministry of Research. Discussions with Andreas Hasler and Ross Purves have helped to develop further the concepts presented here. Thanks to Michi Zemp for his comments on the early manuscript. I acknowledge the valuable input of three anonymous reviewers.

References

Claessens, L., D. Lowe, B. Hayward, B. Schaap, J. Schoorl, and A. Veldkamp (2006), Reconstructing high-magnitude/low-frequency landslide events based on soil redistribution modelling and a late-holocene sediment record from New Zealand, *Geomorphology*, *74*, 29–49.

Evans, I. (1972), General geomorphometry, derivatives of altitude, and descriptive statistics, in *Spatial Analysis in Geomorphology*, edited by R. Chorley, p. 17–92, Mathuen and Co Ltd.

Frauenfelder, R. (2004), Regional-scale modelling of the occurrence and dynamics of rockglaciers and the distribution of paleopermafrost, Ph.D. thesis, University of Zurich, Switzerland.

Freeman, T. (1991), Calculating catchment area with divergent flow based on a regular grid, *Comput. Geosci.*, *17*, 413–422.

Garbrecht, J., and L. Martz (1997), The assignment of drainage direction over fiat surfaces in raster digital elevation models, *J. Hydrol.*, *193*(1–4), 204–213.

Gruber, S. (2005), Mountain permafrost: Transient spatial modelling, model verification and the use of remote sensing, Ph.D. thesis, University of Zurich, Switzerland.

Gruber-Schmid, U., and S. Sardemann (2003), High-frequency avalanches: Release area characteristics and run-out distances, *Cold Reg. Sci. Technol.*, *37*(3), 439–451.

Haeberli, W. (1975), *Untersuchungen zur Verbreitung von Permafrost zwischen Flüelapass und Piz Grialetsch (Graubünden)*, ETH Zurich, Switzerland.

Holmgren, P. (1994), Multiple flow direction algorithms for runoff modeling in grid based elevation models—An empirical evaluation, *Hydrol. Processes*, *8*(4), 327–334.

Huggel, C., A. Kääb, W. Haeberli, and B. Krummenacher (2003), Regional-scale GIS-models for assessment of hazards from glacier lake outbursts: Evaluation and application in the Swiss Alps., *Nat. Hazards Earth Syst. Sci.*, *3*, 647–662.

Huggel, C., W. Haeberli, A. Kääb, D. Bieri, and S. Richardson (2004), An assessment procedure for glacial hazards in the Swiss Alps, *Can. Geotech. J.*, *41*(6), 1068–1083.

Iverson, R. M., S. P. Schilling, and J. W. Vallance (1998), Objective delineation of lahar-inundation hazard zones, *Geol. Soc. Am. Bull.*, *110*(8), 972–984.

Kaser, G., A. Fountain, and P. Jansson (2003), *A Manual for Monitoring the Mass Balance of Mountain Glaciers* (*IHP-VI, Technical Documents in Hydrology, No. 59*), UNESCO, Paris.

Keller, F. (1992), Automated mapping of mountain permafrost using the program permakart within the geographical information system Arc/Info, *Permafrost and Periglacial Processes*, *3*(2), 133–138.

Lea, N. (1992), An aspect driven kinematic routing algorithm, in *Overland Flow: Hydraulics and Erosion Mechanics*, edited by A. J. Parsons and A. D. Abrahams, CRC Press, Boca Raton, Fla.

Lehning, M., J. Doorschot, N. Raderschall, and P. Bartelt (2000), Combining snow drift and SNOWPACK models to estimate snow loading in avalanche slopes, in *Snow Engineering*, edited by H. Hjorth-Hansen, I. Holand, S. Leset, and H. Norem, Balkema, Rotterdam.

Machguth, H., F. Paul, M. Hoelzle, and W. Haeberli (2006), Distributed glacier mass balance modelling as an important component of modern multi-level glacier monitoring, *Ann. Glaciol.*, *43*, in press.

Maggioni, M., and U. Gruber (2003), The influence of topographic parameters on avalanche release dimension and frequency, *Cold Reg. Sci. Technol.*, *37*(3).

Naaim, M., and C. Ancey (1992), Dense avalanche model, *Tech. rep.*, European Summer University, Chamonix, Cemagref, France.

Noetzli, J., C. Huggel, M. Hoelzle, and W. Haeberli (2006), GIS-based modelling of rock-ice avalanches from alpine permafrost areas, *Comput. Geosci.*, *10*, 161–178.

O'Callaghan, J., and D. Mark (1984), The extraction of drainage networks from digital elevation data, *Comput. Vision Graphics Image Process.*, *28*, 323–344.

Park, S., and R. Schowengerdt (1983), Image reconstruction by parametric cubic convolution, *Comput. Vision Graphics Image Process.*, *23*, 258–272.

Plummer, M., and F. Phillips (2003), A 2-D numerical model of snow/ice energy balance and ice flow for paleoclimatic interpretation of glacial geomorphic features, *Quat. Sci. Rev.*, *22*(14), 1389–1406.

Purves, R., W. Mackaness, and D. Sugden (1999), An approach to modelling the impact of snow drift on glaciation in the Cairngorm mountains, Scotland, *J. Quat. Sci.*, *14*(4), 313–321.

Quinn, P., K. Beven, P. Chevallier, and O. Planchon (1991), The prediction of hillslope paths for distributed hydrological modeling using digital terrain models, *Hydrol. Processes*, *5*, 59–79.

Salzmann, N., A. Kääb, C. Huggel, B. Allgöwer, and W. Haeberli (2004), Assessment of the hazard potential of ice avalanches using remote sensing and GIS-modelling, *Nor. Geogr. Tidsskr.*, *58*, 74–84.

Sampl, P., and T. Zwinger (2004), Avalanche simulation with SAMOS, *Ann. Glaciol.*, *38*(1), 393–398.

Schoorl, J., A. Veldkamp, and J. Bouma (2002), Modeling soil and water redistribution in a dynamic landscape context, *Soil Sci. Soc. Am. J.*, *66*, 1610–1619.

Sovilla, B. (2004), Field experiments and numerical modelling of mass entrainment and deposition processes in snow avalanches, Ph.D. thesis, ETH Zurich, Switzerland.

Sovilla, B., F. Sommavilla, and A. Tomaselli (2001), Measurements of mass balance in dense snow avalanche events, *Ann. Glaciol.*, *32*, 230–236.

Tarboton, D. G. (1997), A new method for the determination of flow directions and upslope areas in grid digital elevation models, *Water Resour. Res.*, *33*(2), 309–319.

Winstral, A., K. Elder, and R. Davis (2002), Spatial snow modeling of wind-redistributed snow using terrain-based parameters, *J. Hydrometeorol.*, *3*, 524–538.

S. Gruber, Glaciology and Geomorphodynamics Group, Department of Geography, University of Zurich, Winterthurerstr. 190, 8057 Zurich, Switzerland. (stgruber@geo.unizh.ch)